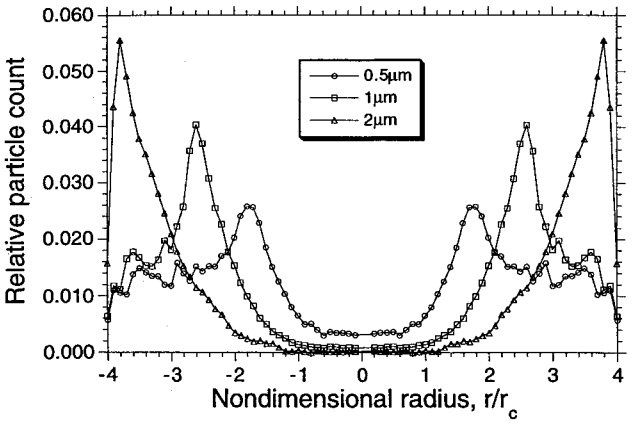

Fig. 4 Computed relative frequency of particles for various particle sizes inside a desingularized vortex, $\Gamma = 5.6\ m^2s^{-1}$.

able picture of the likelihood of being able to successfully seed a vortical flowfield, and also provides an indicator of the data rates and particle weighting count over the measurement grid that one would expect in practice. Data rates are particularly important for rotor tests because of the typically long time scales involved. These particle trajectory calculations were conducted by releasing a large number of uniformly dispersed particles inside the prescribed vortex flowfield at time zero, and integrating the equations of motion in time until the particles spiraled out of the computational grid.

The computed results are shown in Fig. 4 in the form of relative particle count as a function of nondimensional distance from the vortex axis. Note the similarities of these computed results to the measurements shown in Fig. 1. As discussed previously, inside the vortex core ($r/r_c < 1$), the centripetal accelerations cause the particles to spiral quickly outward, creating a seed void. Inside this void, data rates are obviously relatively low, which in practice leads to very long elapsed time frames to acquire measurements to the necessary statistical precision. Note that the particles that are initially released inside the rotational core reach an equilibrium somewhere outside the core, with a much higher overall relative frequency being obtained in these regions. The radial position and magnitude of this peak are strongly dependent on particle size, with the larger particles being centrifuged considerably further outward from the vortex axis.

Conclusions

Experiments and calculations have been conducted to explore issues associated with seeding of strong vortical flows for LDV measurements, such as flows induced by the tip vortices generated by rotors. Both velocity errors and statistical weighting of the seed distribution through the vortex have been examined. Radial velocity errors tend to be larger than swirl errors, and dominate up to two core radii from the vortex axis. The weighting of seed is such that the core (rotational) region suffers a scarcity of particles, with a peak in the density distribution well outside the viscous core. This distribution is very sensitive to particle mass and size. A nondimensional parameter $\hat{A}$ has been developed to help quantify the likelihood of successfully seeding a typical vortex flow.

References

[1]Menon, R., and Lai, W. T., "Key Considerations in the Selection of Seed Particles for LDV Measurements," *Laser Anemometry Advances and Applications*, Vol. 2, *4th International Conference on Laser Anemometry* (Cleveland, OH), 1991, pp. 719–730.

[2]Dring, R. P., "Sizing Criteria for Laser Anemometry Particles," *Journal of Fluids Engineering*, Vol. 104, March 1982, pp. 15–17.

[3]Kriebel, A. R., "Particle Trajectories in a Gas Centrifuge," *Journal of Basic Engineering*, Vol. 83, No. 3, 1961, pp. 333–340.

[4]Leishman, J. G., Baker, A., and Coyne, A., "Measurements of Rotor Tip Vortices Using Three-Component Laser Doppler Velocimetry," *Proceedings of the 2nd International Aeromechanics' Specialists' Conference, American Helicopter Society* (Bridgeport, CT), 1995, pp. 37–57.

[5]Fuchs, N. A., *The Mechanics of Aerosols*, Pergamon, Oxford, England, UK, 1964.

[6]Buchhave, P., George, K. W., and Lumley, J. L., "The Measurement of Turbulence with the Laser Doppler Anemometer," *Annual Review of Fluid Mechanics*, Vol. 11, 1979, pp. 443–503.

[7]Ghee, T. A., and Elliott, J. W., "A Study of the Rotor Wake of a Small-Scale Rotor Model in Forward Flight Using Laser Light Sheet Flow Visualization with Comparisons to Analytical Models," *Proceedings of the 48th Annual Forum of the American Helicopter Society*, Washington, DC, 1992.

Effects of Leading-Edge Sweep Angle on Nonzero Trimmed Roll Angles

Eric J. Stephen* and Drew A. Sopirak†
U.S. Air Force Academy, Colorado 80840

Introduction

RECENTLY, there has been interest in improving aircraft maneuverability through the exploitation of unsteady aerodynamics and thrust vectoring. These techniques can extend the flight envelope to near or even into the poststall flight regime. The extension of the flight envelope increases the need for understanding high-angle-of-attack aerodynamics.

The focus of this study was the roll stability of delta wings at high angle of attack. The symmetry of the delta wing suggests roll stability at 0 deg of roll only, but Hanff and Jenkins[1] showed that at a high incidence angle ($\sigma = 30$ deg) a 65-deg delta wing was statically stable at ±21 deg of roll as well as at 0 deg. Further experiments from Hanff, reported by Jenkins,[2] showed that one-, two-, or three-trimmed roll positions could be produced by changing the model incidence angle. Similar explanations of this phenomenon were provided by Stephen[3] and Ericsson.[4] The current set of experiments was designed to test Stephen's[3] conceptual model and show the effects of sweep angle changes on roll stability.

Free-to-roll experiments were limited to moderately swept delta wing models to avoid wing rock. Three flat-plate delta wing models were tested ($\Lambda = 55$, 60, and 65 deg). The 65-deg model allowed for comparison with previous work.[1,2,4,5] A flat plate 65-deg delta wing with a splitter plate and a scale model F-117 with 67-deg sweep were also tested to determine the effect of more complicated geometries on the trimmed roll positions. Besides the trimmed roll data, examination of the roll trajectories suggested some characteristics of the dynamic flow response.

Methods

Each of the three flat plate models had a root chord length of 10 in. and a thickness of 0.125 in. The leading and trailing edges were beveled from the top and bottom with a 22.5-deg

Presented as Paper 94-1885 at the AIAA 12th Applied Aerodynamics Conference, Colorado Springs, CO, June 20–23, 1994; received July 25, 1995; revision received Feb. 16, 1996; accepted for publication Feb. 16, 1996.

*Frank J. Seiler Research Laboratory, Unsteady Aerodynamics Task Manager; currently Chief, Performance Assessment and Analysis Branch, SBIR Systems Program Office, 185 Discoverer Blvd., Suite 2512, Los Angeles AFB, CA 90245-4695. Member AIAA.

†Cadet, Frank J. Seiler Research Laboratory. Student Member AIAA.

bevel. A mounting shaft, 38 in. long and 0.375 in. in diameter, was attached to the model along the centerline of the model. The other end of the mounting shaft passed through two bearings in the free-to-roll mechanism as shown in Fig. 1. A fairing reduced flow interference from the mounting mechanism. At least one chord length was maintained between the fairing and the trailing edge of the model. The scale model F-117, approximately 10 in. from nose to trailing edge, and the flat plate model with the splitter plate were mounted the same way. The splitter plate model was a modified version of the 65-deg flat plate model. The splitter plate was 0.125 in. thick and 1.0 in. high, beveled at the same angle as the wing and with a leading-edge sweep of 22.5 deg. The splitter plate was mounted perpendicular to the wing along the root chord. For balance, an identical splitter plate was attached to the lower surface.

The free-to-roll rig was bolted to the tunnel floor (Fig. 1). A slot in the floor allowed the mechanism to extend outside the tunnel so that measuring equipment could be connected outside the flow. A Mitutoyo Pro 360 digital inclinometer, with an accuracy of 0.1 deg, was used to set the incidence angle. The roll position was measured using a U.S. Digital E2 optical encoder, providing a maximum position error of ±20 min of arc. The encoder was connected to a personal computer for data acquisition. Data were collected at 50 Hz for 4 s for each run. The low-speed wind tunnel at the U.S. Air Force Academy was used for testing. The wind tunnel had a 3 by 3 ft test section. The tunnel speed was set at 40 ft/s ($Re = 1.6 \times 10^5$, based on chord length). The turbulence level was approximately 0.15%.

A thin, plastic, balance ring was mounted to the rotation shaft outside of the wind tunnel. Small pieces of clay were attached to the ring so that, with no wind, the model remained at any release position.

Free-to-roll tests were performed at incidence angles of 25, 30, and 35 deg. For each test the model was released from offset roll angles from −90 to 90 deg in 5-deg increments to confirm experiment symmetry. Each run was performed three times for repeatability. The trimmed roll positions were recorded and the roll position data for the flat plate models were numerically differentiated to provide motion parameters.

Static Results

The trimmed roll positions from the three initial incidence angle tests were compiled for the three flat plate models in Table 1. For most cases, stability was reached when oscillation damped to ±1 deg. For the 55-deg wing at 25-deg incidence and the 60-deg wing at 30-deg incidence cases, however, the oscillations stabilized on the order of ±10 deg. The trimmed positions were averaged over four oscillation cycles. It was noted that the wing stayed temporarily at some positions before finally settling.

The graph in Fig. 2 shows extended results for a range of incidence angles. For all three sweep angles the final nonzero, trimmed positions appeared as the incidence angle approached the stall angle and decreased in magnitude to zero as the incidence angle increased. The effect of increasing the sweep angle was to increase the minimum incidence angle for nonzero trimmed position to occur. For the 55-deg wing the nonzero trimmed position existed for a very small range of incidence angles. The nonzero trimmed positions occurred either along with or without a trimmed position at 0 deg.[3]

The F-117 model results are shown in Fig. 3 along with the results from the 65-deg flat plate model and the splitter plate model. For the F-117 model, the nonzero trimmed roll points occurred at a lower incidence angle than for the flat plate delta wing. At higher incidence angles the trim points collapsed toward 0 deg like the flat plate model. The minimum incidence angle for the presence of nonzero trim points was nearly the same with or without the splitter plate. The magnitude of the trimmed roll angle for the splitter plate model increased with incidence angles up to 35 deg contrary to the flat plate data. For incidence angles greater than 35 deg, the magnitude of the nonzero trim points decreases rapidly toward zero.

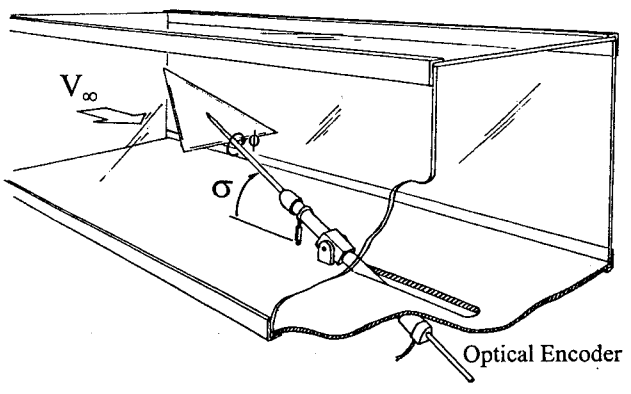

Fig. 1 Free-to roll experimental setup.

Table 1 Trimmed roll positions

Sweep angle, deg	Incidence angle, deg	Trimmed roll angles, deg
65	25	0
	30	±24, 0
	35	−16, 0,[a] 14
60	25	±28, ±14,[a] 0
	30	±18
	35	0
55	25	±38, 0
	30	0
	35	0

[a]The wing remained at these roll angles temporarily.

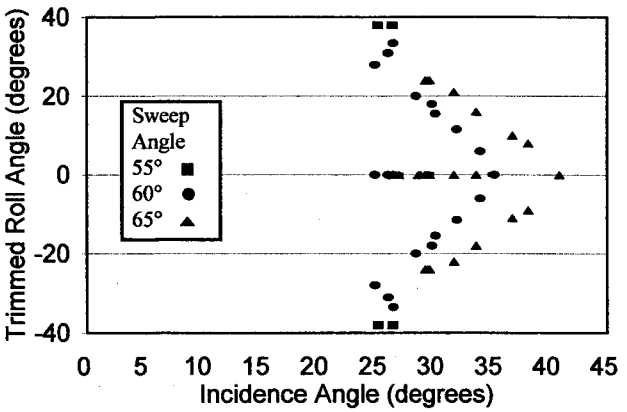

Fig. 2 Nonzero trimmed roll positions for flat plate models.

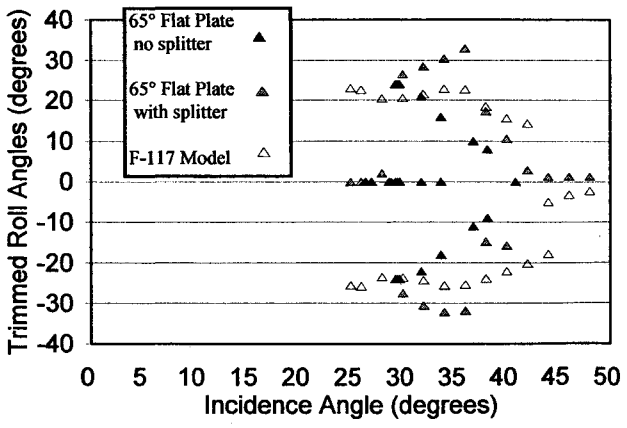

Fig. 3 Nonzero trimmed roll positions for more complicated models.

For a 65-deg swept delta wing model, Hanff et al.[1,2,5] reported nonzero trimmed positions at ±1.5, ±21, and ±11 deg for incidence angles of 25, 30, and 35 deg, respectively. These values differ from the values of 0, ±24, and approximately ±15 deg found in these tests. The difference was suspected to be because of a difference in thickness ratio of the models and the presence of the relatively large centerbody in the tests reported by Hanff. The two sets of data agree, in general, on the trimmed point behavior. Stephen[3] explained this behavior by considering the effective sweep angle on either side of the wing. The combination of roll and incidence angles resulted in an effective angle of attack and sweep angle. Using the effective angles, stall behavior could be predicted to explain the presence of the nonzero trimmed positions. Consistent with this explanation, the sweep effect (Fig. 2) was because of the increase in stall angle with increased sweep angle.

The data for the F-117 model showed that more complicated delta wing geometries also exhibited nonzero trimmed points, but the F-117 data were not simply bounded by the flat plate and splitter plate models. The lack of trimmed point recovery to zero at the highest incidence angles was because of the asymmetric placement of some appendages to the model near the apex.

Dynamic Results

Roll position data from the three trials for each release angle were averaged across the trials. Then averaged roll data were numerically differentiated twice to provide angular acceleration data. Neglecting the friction in the bearing, the rolling moments were calculated by multiplying the angular accelerations by each model's moment of inertia. The calculated rolling moment coefficients were plotted in Fig. 4 vs the instantaneous roll angle for the 65-deg swept model with a 30-deg incidence angle. The data were truncated after the first rolling oscillation to allow the discernment of individual curves. This configuration was also used by Hanff[1] in their forced roll oscillation experiments. After some manipulation, Hanff's rolling moments, measured with a force balance, were also plotted in Fig. 4, for comparison.

The results appear to indicate the independence of the rolling moment from the roll rate, during the initial free rolling movement. After the initial rolling motion, the flowfield and rolling moment began to adjust to the roll conditions, indicated by the departure of the curves from the narrow band, just before truncation. The tight band of rolling moment data passes through zero at the trimmed roll point (−24 deg). Hanff[1] showed the same behavior for the 65-deg delta undergoing forced oscillation. This collapse of dynamic rolling moment data was also apparent for the 60-deg wing at 25-deg incidence (not shown).

In Fig. 5, the dynamic rolling moment data were plotted for the 65-deg swept delta wing, but for incidence angles of 25 deg. The data in Fig. 5 did not collapse into a narrow band like the data in Fig. 4. In Fig. 5 the slope of the curves decreases as the magnitude of the release angle, and the corresponding roll rate, decreases. Ericsson[5] has provided some insight into the difference in behavior. He stated that the pseudosteady behavior of the moment data was because of the fact that the flow structure over the wing remained consistent throughout the motion. Applying this theory to a 30-deg incidence angle case, it is suspected that roll deflections away from zero for the 30-deg incidence angle case increased the effective sweep angle on the leeward side and decreased the sweep on the windward side.[4] The increase forced the burst point aft of the trailing edge on the leeward side and the decrease resulted in flow separation because of the high angle of attack on the windward side. The pseudosteady rolling moment behavior was the result of the burst point remaining off the surface of both sides during the initial rolling motion because of a delay in flow adjustment.

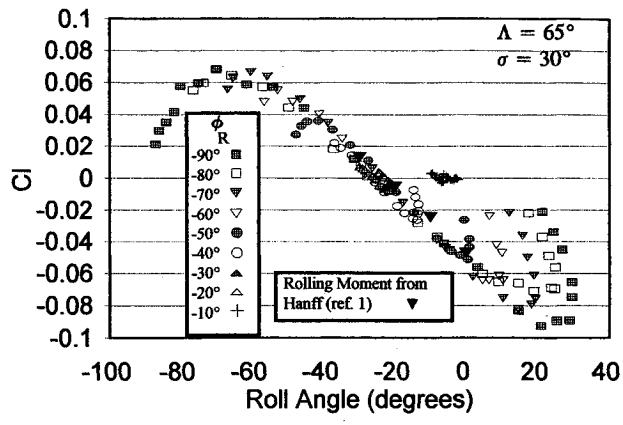

Fig. 4 Dynamic rolling moment data for the 65-deg flat plate model at 30-deg incidence.

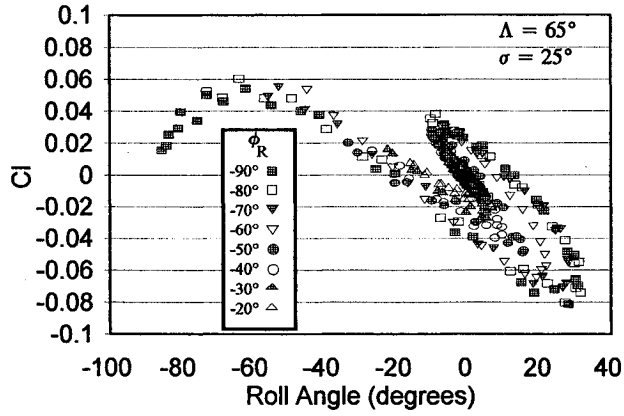

Fig. 5 Dynamic rolling moment data for the 65-deg flat plate model at 25-deg incidence.

For the 25-deg incidence angle case the effective angle of attack was not high enough to force the burst point to the apex on the windward side. The roll rate dependence was caused by the presence of a burst point over windward side. This roll rate dependence was apparent in all of the 60- and 65-deg swept cases except the two noted previously. These results were consistent with the dynamic pressure and force measurements taken on pitching wings by Thompson et al.[6] and Soltani et al.[7] They reported pseudosteady results when delta wings were pitched from low angle of attack into the poststall regime. Pitch rate dependence was shown by Gad-el-Hak[8] and LeMay[9] on pitching delta wings with the burst point over the wing.

Conclusions

Increasing the sweep angle on a delta wing increases the minimum incidence angle where nonzero trimmed roll positions occur. For sweep angles greater than 70 deg wing rock dominates this behavior, but there may also be a lower limit as indicated by the trimmed point behavior for the 55-deg swept wing in these tests.

Free-to-roll tests on an aircraft model produced results similar to those for the flat plate delta wing models. Even though the F-117 model was tested at Reynolds and Mach numbers much less than those for flight, the results indicate these nonzero trimmed roll positions need to be considered in high-angle-of-attack flight.

During the rolling portion of the free-to-roll tests, the unsteady effects were manifested in one of two ways. One way was a time lag in the flow adjustment that was represented by the departure of a set of data from a narrow band of pseudosteady data. The second way was a decrease in the slope of the C_l vs ϕ curve with a decrease in roll rate that was appar-

ently because of the presence of a vortex burst point over the surface.

References

[1]Hanff, E. S., and Jenkins, S. B., "Large Amplitude High-Rate Roll Experiments on a Delta and Double Delta Wing," AIAA Paper 90-0224, Jan. 1990.

[2]Jenkins, J. E., Myatt, J. H., and Hanff, E. S., "Body-Axis Rolling Motion Critical States of a 65-Degree Delta Wing," AIAA Paper 93-0621, Jan. 1993.

[3]Stephen, E. J., "Analysis of Rolled Delta Wing Flows Using Effective Sweep and Attack Angles," *Journal of Aircraft*, Vol. 32, No. 5, 1995, pp. 978–984.

[4]Ericsson, L. E., "Flow Physics of Critical States for Rolling Delta Wings," *Journal of Aircraft*, Vol. 32, No. 3, 1995, pp. 603–610.

[5]Ericsson, L., and Hanff, E., "Further Analysis of High-Rate Rolling Experiments of a 65 Deg Delta Wing," AIAA Paper 93-0620, Jan. 1993.

[6]Thompson, S., Batill, S., and Nelson, R., "Unsteady Surface Pressure Distributions on a Delta Wing Undergoing Large Amplitude Pitching Motions," AIAA Paper 90-0311, Jan. 1990.

[7]Soltani, M. R., Bragg, M. B., and Brandon, J. M., "Measurements on an Oscillating 70-Deg Delta Wing in Subsonic Flow," *Journal of Aircraft*, Vol. 27, No. 3, 1990, pp. 211–217.

[8]Gad-el-Hak, M., and Ho, C.-M., "The Pitching Delta Wing," *AIAA Journal*, Vol. 23, No. 11, 1985, pp. 1660–1665.

[9]LeMay, S. P., Batill, S. M., and Nelson, R. C., "Vortex Dynamics on a Pitching Delta Wing," *Journal of Aircraft*, Vol. 27, No. 2, 1990, pp. 131–138.

Comparative Study of Delta Wings with Blunt Leading Edges and Vortex Flaps

Lance W. Traub*
Texas A&M University, College Station, Texas 77843

Introduction

STUDIES of slender delta wings have typically used models that are usually thin and consequently sharp edged. This leading-edge configuration is usually viewed as representing the best compromise in terms of supersonic performance, since linearized theory suggests that a sharp edge minimizes the zero lift wave drag penalty. However, as long as the wing's leading edge is subsonic (i.e., the Mach number normal to the leading edge is less than unity) and sufficiently rounded, leading-edge suction is developed, even if not at the level suggested by theory.[1] As shown in Ref. 2, nonlinear flow codes (and experiment) show that leading-edge bluntness has a small effect on zero lift wave drag, and additionally reduces the drag from lift compared to a sharp wing as long as the wing's leading edge is subsonic. In subsonic flow (and to a lesser extent supersonic flow) a sharp leading edge may be beneficial in that the enforced flow separation occurring at the wing's leading edge, results in a substantial increase in lift because of the suction of the leading-edge vortices that form. However, as shown by Polhamus,[3] lift enhancement effects are necessarily at the expense of a drag penalty because of the loss of leading-edge suction. Thus, not only is leading-edge thrust diminished, but after effective rotation[3] through 90 deg to supplement the normal force coefficient, it contributes to drag.

Recent studies[4–6] have shown the leading-edge vortex flap LEVF (and numerous variations thereof[7–9]) to be an effective solution to the major drawback of slender sharp-edged deltas as detailed previously. An effective vortex flap works by concentrating the suction of the leading-edge vortex on the flap so that when suitably deflected, a component of the vortex-induced suction acts as thrust. Performance improvements because of LEVFs are consequently attributed to this wing configuration generating an axial force component, i.e., thrust. In general, studies of vortex flaps usually compare the performance of the wing equipped with flaps to a planar sharp-edged equivalent, or the test configuration without the flaps, but still sharp edged. This is obviously a meaningful comparison if effects of deflecting a LEVF on an existing sharp-edged wing are to be studied. However, a more complete representation of LEVF effectiveness may be gauged by comparing the wing with a LEVF to a geometrically similar blunt-edged wing, which is thus also capable of generating leading edge thrust. In this Note, comparisons are made between vortex flap data, and that for a similar blunt-edged wing.

Discussion

The following discussion compares results from the three experimental investigations described next. All of these studies were conducted at low speed.

Reference 10 contains a study by Bartlett and Vidal that details the effect of leading-edge shape on the aerodynamic characteristics of various symmetrical low-aspect ratio wings. As may be expected, the results showed that a blunt leading edge delayed crossflow separation on the delta wings that were studied. It was also shown that for the Reynolds number Re of the tests (3 and 6×10^6) an elliptic leading edge showed less sensitivity to this parameter than a round leading edge. Generally, performance was seen to improve at the higher Reynolds number.

Levin and Seginer,[4] in an investigation of vortex flaps on delta wings, showed that there is in general no optimal flap deflection angle δ_F for best performance, but an optimum for a specific incidence. This required flap angle increased as angle of attack α increased. They also showed that the specific shape of the leading edge had little influence (all were sharp edged). Rinoie and Stollery[5] in a study of vortex flaps and vortex plates showed that maximum lift-to-drag occurred when there was smooth onflow onto the flap, with no separation. It was also found that a vortex plate has analogous performance to a leading-edge vortex flap.

All of the following data comparisons are made for a vortex flap deflection angle of 30 deg, as this deflection angle has been shown to be effective,[5] and represents optimal LEVF performance over a reasonable lift coefficient C_L range. Details of the three models compared are given in Table 1.

Figure 1 presents C_L as a function of angle of attack. Also included on the plot are results for a sharp-edged planar delta of AR = 2 determined using the method of Polhamus[3] (i.e., no thrust + vortex lift). Results are also included for 100% leading-edge suction (i.e., elliptic loading) and thus full thrust. The substantial theoretical lift enhancement effects caused by vortex lift are clearly shown. Good correlation is shown between the full thrust curve and the results of Bartlett and Vidal.[10] This figure also shows the cambering effect of LEVF deflection. Although on a sharp-edged delta wing flap deflection decreases vortex lift (mainly because of a suppression of vortex formation) for a given incidence, it may be seen that lift increases more rapidly for the LEVF configurations than the blunt-edged wing because of vortex suction. Figure 1 does demonstrate that at high lift coefficient, even with $\delta_F = 30$ deg, lifting performance for the LEVF models is superior to the blunt-edged wing.

Received Nov. 12, 1995; revision received Feb. 13, 1996; accepted for publication Feb. 19, 1996.

*Graduate Student, Aerospace Engineering Department. Associate Member AIAA.